Acta Pharmaceutica Sinica B 2025;15(6):2900−2914

Chinese Pharmaceutical Association
Institute of Materia Medica, Chinese Academy of Medical Sciences

Acta Pharmaceutica Sinica B

www.elsevier.com/locate/apsb
www.sciencedirect.com

ORIGINAL ARTICLE

Submicron-sized superantigen biomimetic liposomes with highly efficient pulmonary accumulation to remodel local immune microenvironment for cancer chemoimmunotherapy

Bochuan Yuan[a,b], Feng Zhang[b], Qiucheng Yan[b], Wanmei Wang[b], Zhangyu Li[b], Lina Du[b], Yiguang Jin[b,*], Fei Xie[a,*]

[a]*College of Pulmonary and Critical Care Medicine, Chinese PLA General Hospital, Beijing 100048, China*
[b]*Beijing Institute of Radiation Medicine, Beijing 100850, China*

Received 14 November 2024; received in revised form 2 February 2025; accepted 12 February 2025

KEY WORDS

Metastatic lung cancer;
Chemoimmunotherapy;
Bacterial superantigen;
Biomimetic liposome;
Lung targeting;
Immune microenvironment;
Submicron liposome;
Immunosuppression reversal

Abstract Metastatic lung cancer continues to cause a high number of deaths due to high malignancy and poor prognosis, and the efficacy of typical chemotherapy or immunotherapy is less than ideal due to the low pulmonary accumulation and targeting of therapeutics. Here, a submicron-sized biomimetic liposome was formulated for the lung-targeted co-delivery of bacterial superantigen and paclitaxel. Recombinant staphylococcal enterotoxin C2 (rSEC2), a bacterial superantigen, was expressed with the *Escherichia coli* system and showed potent immunostimulatory activities to mediate tumor cell death. The submicron-sized (∼800 nm) biomimetic liposomes, namely 4T1 cell membrane-hybrid rSEC2 paclitaxel liposomes (TSPLs), exhibited high lung-accumulation efficiency and tumor homologous effect due to the suitable particle size and membrane hybridization of cancer cell membranes with phospholipids. Intravenous TSPLs remarkably inhibited metastatic lung cancer with limited systemic immune responses. TSPLs reversed the immunosuppressive state and increased the proportion of local $CD4^+$ and $CD8^+$ T cells in the lung; moreover, paclitaxel increased tumor cell apoptosis and reduced tumor burden. In summary, the high lung cancer targeting was achieved by particle size control and cell membrane hybridization, and the highly efficient anticancer effect was achieved by the co-delivery of superantigens and chemotherapeutic drugs.

*Corresponding authors.
E-mail addresses: jinyg@sina.com (Yiguang Jin), xiefei0522@163.com (Fei Xie).

Peer review under the responsibility of Chinese Pharmaceutical Association and Institute of Materia Medica, Chinese Academy of Medical Sciences.

https://doi.org/10.1016/j.apsb.2025.03.019

1. Introduction

Cancer continues to claim lives and has emerged as one of the principal causes of human mortality globally. Lung cancer is the leading cause of cancer mortality in males and is the second leading cause in females, surpassed only by breast cancer, with an estimated 2.2 million new cases and 1.8 million deaths in 2020[1]. The lung represents the most prominent target organ for cancer metastasis, with metastatic lung cancer occurring in 20%−54% of patients diagnosed with metastatic malignancies[2]. Systemic chemotherapy is a common treatment modality for lung metastases. However, due to issues with pulmonary accumulation and targeting, its efficacy is less than ideal[3]. The organ targeting is primary for lung cancer, followed by drug release and delivery in the microenvironment[4,5]. The modification of drug delivery carriers with bioactive materials significantly improves drug distribution, where various toolkits are used to enhance cancer targeting, such as ligand-receptor binding, homologous biomembrane affinity, and polymer molecular motors[6-8]. The complex multimolecular modified delivery carriers increase the difficulty of drug clinical translation, therefore, the control of the physical properties of carriers is recommended to achieve lung targeting.

Liposomes have shone brilliantly in recent years, particularly during the COVID-19 pandemic[9-11]. Tumor-targeted liposomes have been proven to enhance drug bioavailability and reduce side effects[12-14], yet improving the tumor-targeting capability of liposomes remains a challenge. Cell membrane-modified liposomes represent an emerging class of nanocarriers[15], yielding biomimetic nanoformulations with several properties typically associated with the source cell, including improved biocompatibility, immune evasion, and tumor targeting[16-19]. The bio-interface provided by the cell membrane is enriched with membrane proteins, which confers a stronger affinity for homologous cells[20,21]. However, cell membrane-mediated tumor targeting represents a passive approach that relies on accumulating nanoformulations at the tumor site. Despite the enhanced permeability and retention (EPR) effects of liposomes leading to their retention in the body for a long time[22,23], particles below 500 nm tend to indistinguishably accumulate in the liver[24,25]. Liposomes mostly accumulate in the reticuloendothelial system organs, such as the liver, spleen, and lung, within 15−30 min after intravenous administration[26]. In general, liposomes with a particle size >5 μm can be passively retained by the vascular network of the lung[27,28]. The poly(lactic-*co*-glycolic acid) (PLGA) microspheres with a diameter of 12 μm displayed almost exclusive distribution to the lungs[29]. Nevertheless, solid and micron particles pose a risk of causing pulmonary embolism[30]. Particles with a size of <1 μm are particularly attractive, based on a combination of various lung-targeting strategies[26]. An anti-ICAM-1 antibody-modified nanoparticle achieves efficient lung targeting with a particle size of 237 nm[31], while the size effect of cell membrane-modified liposomes on lung targeting has not yet been explored.

The immunotherapies utilize the power of leveraging the immune system in the fight against cancer and have achieved success in fields, including immune checkpoint inhibitors, chimeric antigen receptor (CAR) T-cell therapy, cancer vaccines, and immunomodulators[32,33]. Bacterial superantigens, as a typical immunomodulator, have significant potential in the treatment of cancer[34,35]. They are produced by only a few bacteria, among them, staphylococcal enterotoxins (SEs) produced by *Staphylococcus aureus*, are one of the most studied and fully elucidated bacterial superantigens[36]. At present, two drugs with SE as the main component have been approved for marketing in China for adjuvant treatment of cancer[37]. The excellent anti-tumor activity of SEs is attributed to sufficient stimulation for T lymphocytes. *In vitro,* femtomolar concentrations of SEs can stimulate profound proliferation and cytokine production in up to 20% of all peripheral T cells[38-40]. However, due to the organ accumulation issues and targeting challenges, SEs are prone to induce systemic cytokine storms leading to a toxic shock syndrome[41]. The local accumulation of SEs within tumors holds promise for recruiting a large number of T cells at the tumor site while limiting systemic side effects.

Chemotherapy and immunotherapy have respectively represented the classical methods and emerging modalities for the treatment of pulmonary metastases over the past decades[42]. Nevertheless, the former generally exhibits poor targeting and may result in immunosuppression, while the clinical response rate (∼20%) of the latter is far from satisfactory[43,44]. Furthermore, immunomodulators such as SEs are considered to be solely applicable as adjuvant therapy for cancer[45,46]. Therefore, a new chemoimmunotherapy strategy that integrates the advantages of immunotherapy and chemotherapy has currently emerged as a more promising therapeutic approach for cancer treatment[47].

In this study, we explored a submicron-sized biomimetic bacterial superantigen liposome for chemoimmunotherapy of breast cancer lung metastasis. Simultaneous lung targeting of superantigen and chemotherapeutic agent (paclitaxel) was achieved through the concise submicron-sized biomimetic liposomes. Our data demonstrated that the superantigen-loaded biomimetic paclitaxel liposome mediates a high level of antitumor immune response locally in the lung, avoiding systemic inflammatory storm, and paclitaxel further kills lung cancer cells. Our study provides a new targeting strategy for chemoimmunotherapy of lung metastasis, and the formulation has prospects for medical translation due to its simple preparation process.

2. Materials and methods

2.1. Materials

The *Escherichia coli* (*E. coli*) DH5α and BL21 (DE3) competent cells, BM2000+ DNA Marker were purchased from Beijing Biomed Gene Technology Co., Ltd. (Beijing, China). Q5 DNA polymerase, SspI, and T4 polymerase were purchased from New England BioLabs Company (Ipswich, UK). Mouse IFN-γ, IL-2, IL-4, and IL-10 ELISA kits were purchased from Shanghai Enzyme-linked Biotechnology Co., Ltd. (Shanghai, China). A murine lymphocyte separation kit, and Luria−Bertani (LB) culture medium were purchased from Solarbio Biotech. Co., Ltd. (Beijing, China). Egg yolk lecithin (EPC) and cholesterol were

bought from AVT (Shanghai) Pharmaceutical Technology Co., Ltd. (Shanghai, China). Sephadex LH-20 was purchased from GE HealthCare Technologies Inc. (Chicago, IL, USA). RPMI 1640 culture media, trypsin-ethylene diamine tetraacetic acid (EDTA), and fetal bovine serum (FBS) were purchased from Gibco Life Technologies (Carlsbad, CA, USA). Cell counting kit-8 (CCK-8) was purchased from DOJINDO Laboratories (Kumamoto, Japan). The CD44, CD47, EpCAM, and β-actin antibodies were purchased from Servicebio Biotechnology Co., Ltd. (Wuhan, China).

2.2. Cells and animals

Luciferase labeled 4T1 (4T1-luc) cells, and 4T1 cells (a mouse breast cancer cell line) were purchased from the Cell Bank of the Chinese Academy of Sciences (Shanghai, China), and cultured in the RPMI 1640 supplemented with 10% FBS at 37 °C with a humidified 5% CO_2 atmosphere. L929, HT29, and RAW264.7 cells were deposited in the laboratory, and cultured following previous methods[47,48].

Female BALB/c mice (18−20 g) were provided from Beijing Vital River Laboratory Animal Technology Co., Ltd. (Beijing, China). They were housed under the constant conditions of humidity (50 ± 5%) and temperature (25 ± 1 °C) with 12−12 h light−dark cycles. Food and water were available *ad libitum*. All experimental procedures were approved by the Animal Care and Use Committee of the Beijing Institute of Radiation Medicine and complied with the principles of laboratory animal care and use guidelines.

2.3. Expression and purification of recombinant SEC2

The SEC2 gene was synthesized according to the GenBank record (accession number: 1CQV_A). The gene was introduced into pMCSG7 by previously reported ligation-independent cloning (LIC) method[49], to generate pMCSG7-SEC2. The super fold green fluorescent protein gene (sfGFP) was amplified from pT7-sfGFP and recombined into pMCSG7-SEC2 to generate pMCSG7-SEC2-sfGFP. Both plasmids were verified by sequencing and transformed into *E. coli* BL21 (DE3) for protein expression. The pMCSG7-SEC2 and pMCSG7-SEC2-sfGFP were used for producing recombinant SEC2 (rSEC2) and green fluorescence-labeled rSEC2 (GS). The protein expression and purification process followed the previous report[50]. The purity of rSEC2 was analyzed by SDS-PAGE. The protein content of rSEC2 was determined by bicinchoninic acid (BCA) protein assay and stored at −80 °C.

2.4. Western blotting and MALDI-TOF-MS

Different samples were mixed with loading buffer for sodium dodecyl sulfate-polyacrylamide gel electrophoresis (SDS-PAGE). The proteins in the gel were transferred onto polyvinylidene fluoride membranes and then blocked with 5% non-fat powdered milk (in TBST). The membrane was incubated with CD44, CD47, EpCAM, and β-actin antibodies (all antibodies were diluted at 1:5000) as the primary antibody overnight at 4 °C. Then, the membrane was incubated with anti-mouse IgG conjugated to horseradish peroxidase (HRP, diluted at 1:3000) for 1.5 h for imaging (Guangzhou light instrument Biotechnology Co., Ltd., Ol600MF Plus, Guangzhou, China). The purified rSEC2 solution was added to sinapic acid for drying, then the dried sample was measured by an AB SCIEX TOF/TOF5800 system (Applied Biosystems, Inc., AB SCIEX TOF/TOF5800, Milwaukee, WI, USA).

2.5. Immunostimulatory activity assays of rSEC2

The splenic lymphocytes from mice were isolated using the murine lymphocyte separation kit and counted by a cell counter (Shanghai Ruiyu Biotechnology Co., Ltd., Countstar IC1000, Shanghai, China). Lymphocyte density was adjusted to 1×10^5 cells/well, then rSEC2 was added at various concentrations from 1 μg/mL to 10 μg/mL. After 24 h co-incubation, 10% CCK-8 solution was added. The optical density (OD) at 450 nm was recorded by a microplate reader (Tecan Trading AG, Spark, Männedorf, Switzerland). Cell viabilities were calculated as Eq. (1):

$$\text{Cell viability}\ (\%) = \left(\text{OD}_{\text{sample}} - \text{OD}_{\text{blank}}\right) \Big/ \left(\text{OD}_{\text{control}} - \text{OD}_{\text{blank}}\right) \times 100 \quad (1)$$

For *in vitro* assay of tumor cell proliferation inhibition, 4T1-luc cells (3.125×10^3 cells/well in a 96-well plate) were added to the aforementioned co-incubation product of splenic lymphocytes and rSEC2. After 24 h incubation, the cell supernatant and suspended cells were removed, and the fresh medium with 10% CCK-8 solution was added to the remaining viable cells for a 1-h incubation. Cell viability was calculated using the same method.

2.6. Formulations preparation

SEC2 liposomes (SLs) were prepared by reverse evaporation (RSLs) and freeze-drying (DSLs) methods. RSLs: Phosphatidylcholine and cholesterol were dissolved in absolute ethyl ether. rSEC2 containing phosphate buffer solution (PBS, pH7.4) was added for hydration after a film forming. The uniform emulsion liquid was the RSLs. DSLs: The process was similar to RSLs preparation, but the hydration solution did not contain rSEC2. After adding the mannitol solution, the uniform emulsion liquid was freeze-dried to obtain the blank liposomes. rSEC2 (500 μg) solution was added to the freeze-dried products and incubated for 30 min at 37 °C, and then extruded through 0.22 μm filters.

The 4T1 cells were cultured, and dispersed in membrane extraction buffer solution A. Then, the membranes were collected using a Membrane Protein Extraction Kit. The mixture was centrifuged (700×*g*, 10 min, 4 °C), and the supernatant was further centrifuged at 14,000×*g* for 30 min (Thermo Fisher Scientific Co., Ltd., Sorvall Legend Micro 21R, Waltham, MA, USA). The extracted cell membranes (TMs) were quantified by the bicinchoninic acid (BCA) protein quantitation method. The purified membranes were mixed with SLs with 500 μg/mL rSEC, and through the polycarbonate membrane with the pore size of 200 nm to prepare TSLs.

For liposome size control, a Sephadex® column (LH-20) was used for liposome separation, and the initial eluate was collected to obtain large-sized liposomes, following the aforementioned SLs preparation process to obtain ~800 nm SLs (SL-800). The ratio of SL-800 to total liposomes was approximately 1:7. The extracted 4T1 cell membranes were mixed evenly with SL-800 suspension, and then co-extruded 3 times using a liposome extruder (ATS, AE001, Suzhou, China) with a 1-μm polycarbonate semipermeable membrane to prepare TSL-800. For formulations visualization, the rSEC2 was replaced with GS to obtain various green fluorescence-labeled formulations, including green fluorescence-labeled SEC liposomes (GSLs), 4T1 cell membrane hybrid GSLs (TGSLs), and larger particle size GSL-800, TGSL-800. In the initial stage of the preparation of TSL-800, paclitaxel (Fujian South Pharmaceutical Co., Ltd.,

Sanming, China) was added to the formulation, then following the aforementioned process to obtain 4T1 cell membranes hybrid rSEC2 paclitaxel liposomes (TSPLs).

2.7. Circular dichroism spectrum, size, zeta potential, and TEM of formulations

RSLs and FSLs were disrupted using 1% Triton X-100 to obtain the loaded SEC2. The rSEC2 and the denatured SEC2 (dSEC2, boiled in water for 10 min) were used as the positive and negative controls, respectively. The circular dichroism (CD) spectra of the four samples mentioned above were detected using a spectrometer (JASCO Corporation, J-1500, Tokyo, Japan).

The size and zeta potential of formulations were determined with the dynamic light scattering (DLS) method on Zetasizer (Malvern Instruments Inc., Nano ZS, Malvern City, UK). The morphology of formulations was inspected using a transmission electron microscope (TEM) (Hitachi Co., Ltd., H-7650, Tokyo, Japan) after staining with 2% sodium phosphotungstate solutions.

2.8. Hemolysis assay

The hemolysis assays of formulations were conducted with rat red blood cells (RBCs). Briefly, a 2% RBC suspension was mixed with different formulations, PBS (negative control), and 1% Triton X-100 solutions (positive control) at 37 °C for 2 h, respectively. After the suspensions were centrifuged at 2000 rpm in a centrifuge (Thermo Scientific), the OD_{540} of supernatants was measured using a microplate reader. The hemolysis rates were calculated according to Eq. (2):

$$\text{Hemolysis rate } (\%) = (OD_{sample} - OD_{negative})/(OD_{positive} - OD_{negative}) \times 100\% \quad (2)$$

2.9. Formulations safety evaluation

The L929 cell toxicity of the formulations with different rSEC2 concentrations was evaluated using the CCK-8 method. L929 cells (1×10^4 cells/well) were seeded in 96-well plates and incubated overnight. Different concentrations of rSEC2, SL, and TSL were added following 24 h co-incubation. Then, CCK-8 reagents were added and the cell viability was calculated following the aforementioned method.

The mice ($n = 5$) were injected with PBS and various formulations with a rSEC2 dose of 4 mg/kg, and another group without any treatment was defined as negative control (NC). The mice were sacrificed after being administered once a day for three consecutive times, and their blood was collected for serum Aspartate aminotransferase (AST), Alanine aminotransferase (ALT), blood urea nitrogen (BUN), and creatinine (CREA) detection following manufacturer's manuals.

2.10. Co-localization of formulations and cells

RAW264.7, HT29, L929, and 4T1-luc cells were cultured to the logarithmic growth phase for trypsin digestion and then seeded into 12-well plates (1×10^5 cells/well) for 24-h incubation at 37 °C. TGSLs (1 μg/mL) were added to the wells, followed by a 4-h incubation at 37 °C. The supernatants of the cell cultures were discarded, and then Dil and DAPI staining were performed for laser confocal imaging (Nikon, TiE-A1, Tokyo, Japan).

2.11. In vivo imaging and rSEC2 quantification

Mouse models of metastatic lung cancer were established and referred to the previous reports[51,52]. Briefly, the 4T1 cells (2×10^5) were intravenous (i.v.) injected into the female mice, and the lungs were separated to test the success of the model after 2 weeks. The mice were randomly separated into different groups to i.v. with 4 mg/kg of GS, GSLs, TGSLs, GSL-800, and TGSL-800, respectively. The main organs, including the heart, liver, spleen, lung, and kidney, were dissected out after 1, 4, and 12 h after injection for *in vivo* imaging using an *in vivo* imaging system (IVIS) (Tanon, ABL-X5, Shanghai, China). The lungs were homogenized for rSEC2 quantification using the enterotoxin ELISA kit according to the manufacturer's manual.

2.12. Model, administration, and treatment

The metastatic lung cancer model was established following the above method. The mice were randomly assigned to 8 groups ($n = 7$), *i.e.* the healthy, model, rSEC2, SL, SL-800, TSL-800, paclitaxel liposome (PL), and TSPL. The mice began to receive treatment on Day 3 after modeling and were administered formulations once every other day for a total of three times. All rSEC2-containing formulations were i.v. injected with a dose of 4 mg/kg rSEC2, while all paclitaxel-containing formulations were i.v. injected with a dose of 10 mg/kg paclitaxel. The mice weight, final lung weight, and final spleen weight were recorded every other day until the end of the experiment. On Day 21 after modeling, the mice were sacrificed for blood white blood cells (WBCs) counting (DYMIND, DF52-Vet, Shenzhen, China), biochemical analyses of the lung and spleen. The spleen index was defined as Eq. (3):

$$\text{Spleen index} = \text{Weight of spleen (mg)} / \text{Weight of mouse (g)} \quad (3)$$

2.13. Histopathologic examination

The upper lobes of the right lung were excised and fixed with 4% paraformaldehyde for 24 h, followed by paraffin embedding, sectioning, hematoxylin−eosin (H&E), and terminal deoxynucleotidyl transferase dUTP nick end labeling (TUNEL) staining. The pathological sections were observed under a microscope (Invitrogen, EVOS M5000, Waltham, MA, USA).

2.14. Immunofluorescence of lung tissue sections

The left mice's lungs were embedded in paraffin. The sections were deparaffinized, rehydrated, and microwave-heated for 15 min in the EDTA antigen retrieval solutions (pH 8.0) for antigen retrieval. The CD4 and CD8 immunofluorescence probes were used to detect the differentiated lymphocytes in the lung sections. The F4/80 and CD206 immunofluorescence probes were used to detect TAMs in the lung sections. The images of the above sections were recorded on a fluorescent microscope (Nikon). The ImageJ was used to quantify the fluorescence intensity of each group of sections.

2.15. ELISA detection

The upper lobes of the left lungs and the spleens were homogenized using a tissue homogenizer (Servicebio, KZ-II, Wuhan, China) at 60 Hz for 5 min. Then, the homogenates were

centrifuged at 5000×*g* and 4 °C for 10 min, and the supernatant was collected for ELISA detection. IL-2, IL-4, IL-10, and IFN-γ levels were detected using the ELISA kits according to the manufacturer's instructions.

2.16. Statistics

Statistical analysis and graphical output of the data were performed with GraphPad Prism (GraphPad Software Company, v 8.0.2, Boston, MA, USA). Single comparisons were made using unpaired two-tailed *t*-tests. Multiple comparisons were analyzed using one-way or two-way analyses of variance (ANOVA).

3. Results

3.1. Immunostimulatory effect of rSEC2

Due to the low natural production of SEC2 in *S. aureus* and the difficulty of purification, we used the classical *E. coli* expression system to recombinant express rSEC2. The *sec2* gene was synthesized according to the previously reported sequence and cloned into the pMCSG-7 expression vector[53]. The pMCSG-7-sec2 plasmid was transformed into the *E. coli* BL21 strain for protein expression, and the purified rSEC2 was obtained by one-step Ni-NTA affinity column purification (Fig. 1A). The purified rSEC2 was digested by TEV protease to remove His_6 tag for SDS-PAGE and MS analyses. The purified rSEC2 showed high purity and expected molecular weight (27.9 kD) according to the SDS-PAGE and MS results (Fig. 1B and C).

To verify the biological activity of the obtained rSEC2, the mouse spleen lymphocytes were extracted for proliferation index (PI) test and cytokines quantification induced by rSEC2. After co-incubation with rSEC2, the PI of the mouse spleen lymphocytes was significantly increased in a dose-dependent way, compared to negative control (Fig. 1D), demonstrating the excellent T cell activation activity of rSEC2. The levels of IFN-γ, IL-2, IL-4, and IL-10 of the stimulated spleen lymphocytes also increased significantly, indicating that rSEC2 significantly induces immune cell differentiation and release of inflammatory factors (Fig. 1E–H). Among them, the significant increase in IL-10 mediated by rSEC2 was noteworthy, as the role of IL-10 in

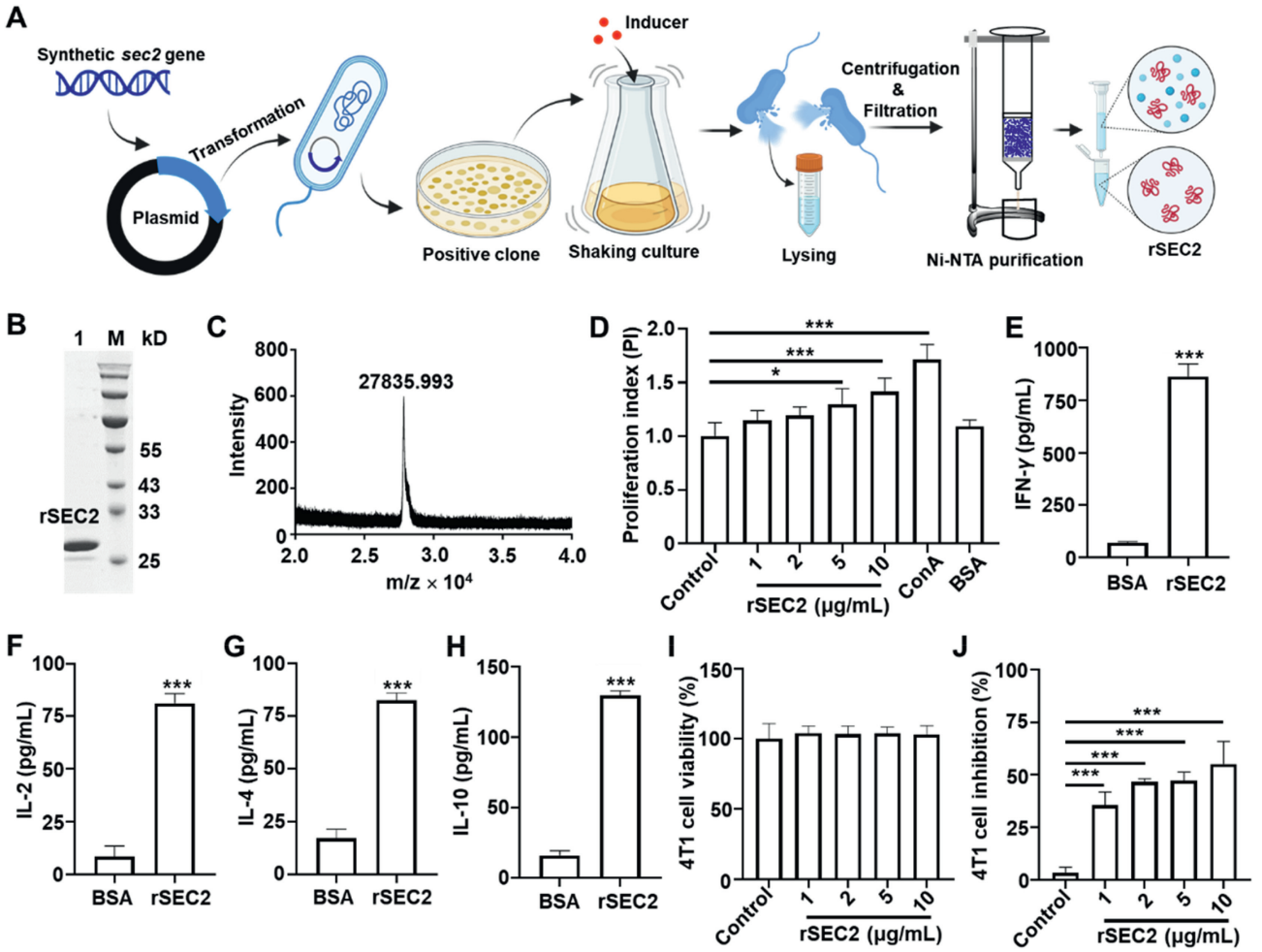

Figure 1 Preparation and characteristics of rSEC2. (A) Preparation procedure of rSEC2. SDS-PAGE analysis (B) and MS (C) of rSEC2. (D) Proliferation index (PI) of mouse spleen lymphocytes after treatment with various concentrations of rSEC2. IFN-γ (E), IL-2 (F), IL-4 (G), and IL-10 (H) levels of mouse spleen lymphocytes after rSEC2 treatment. (I) 4T1 cell viability after treatment with various concentrations of rSEC2. (J) 4T1 cell inhibition rate after treatment with various concentrations of rSEC2, when adding mouse spleen lymphocytes to the culture system. Data are presented as mean ± SD ($n = 3$), $^{*}P < 0.05$, $^{***}P < 0.001$.

antitumor immunity was complex. The inhibitory activity of rSEC2 on the proliferation of 4T1 cells, a mouse breast tumor cell line, was evaluated. Interestingly, rSEC2 did not affect the proliferation of 4T1 cells (Fig. 1I), while when the mouse spleen lymphocytes were added to the mixture, rSEC2 showed a dose-dependent inhibitory effect on 4T1 cell proliferation (Fig. 1J), indicating rSEC2 as an immune modulator exert antitumor effects by activating lymphocytes. Thereby, we obtained high-purity rSEC2 with high immunostimulatory activity through recombinant expression.

3.2. Characteristics of tumor cell membrane-hybrid biomimetic liposomes

To improve the antitumor effects of rSEC2, we anticipated improving the distribution of rSEC2 at the tumor site by using biomimetic liposome hybridized with homologous tumor cell membranes as a vehicle. rSEC2 loaded liposomes (SL) were first prepared and then co-extruded with tumor cell membranes to obtain hybrid biomimetic liposomes. However, due to the poor tolerance of proteins to organic solvents, we prepared SLs using the reverse-phase evaporation (RSLs) and freeze-drying (FSLs) methods and compared the differences in CD spectrum between the two liposomes to evaluate the maintenance of rSEC2 structure. FSL was derived from blank liposomes through lyophilization, followed by reconstitution with rSEC2 solution (Fig. 2A). FSLs exhibited a CD spectrum comparable to that of rSEC2, whereas RSL displayed a CD spectrum analogous to that of denatured SEC2 (dSEC2), indicating FSL retained the active SEC2 (Fig. 2B).

Given the metastatic lung cancer model in this study was generated by the 4T1 breast cancer cells, tumor cell membranes (TMs) were extracted from 4T1 cells to prepare targeting rSEC2-loaded liposomes (TSLs). The diameters of SL and TSL were both ∼200 nm, with TSL being marginally larger than SL (Fig. 2C). SL, TSL, and TM all exhibited negative electrical charge (Fig. 2D) and were quasi-spherical in morphology (Fig. 2E). The size distribution of TSL exhibited a uniform normal distribution (Fig. 2F). To characterize the proteins on the cell membrane surface, SDS-PAGE and Western blotting were respectively performed on 4T1 cells, TM and TSL. After staining with Coomassie Brilliant Blue G-250, all three samples exhibited a multitude of protein bands with varying molecular weights (Fig. 2G). TSL demonstrated a distinct band corresponding to rSEC2, indicating a high loading of rSEC2. CD47 is expressed on the surface of cancer cells, which are considered as a receptor protecting cancer cells from the host immune system[54]. CD44 and EpCAM respectively denoted the glycoproteins and epithelial adhesion molecules that are highly expressed on the surface of malignant tumor cells, which participate in cell−cell interaction, cell adhesion, and cell migration[55,56]. Using β-actin as a control, we specifically identified CD44, CD47, and EpCAM on TSL. All three key surface proteins exhibited good retention in TSL (Fig. 2H), indicating their superior tumor-targeting capability.

The stability and safety of the cell membrane hybridized SEC2 liposomes were evaluated. Three samples of TSL were placed at 4 °C and monitored for changes in particle size and zeta potential for 7 consecutive days. It was found that the particle size fluctuated within a small range while the potential slightly decreased (Fig. 2I), indicating good stability of the formulation. The hemolysis test showed that rSEC2 and its formulations did not cause a hemolysis rate higher than 0.5% (Fig. 2J), indicating that the formulations have good blood compatibility and can be administered intravenously. Although the above experiments verified that rSEC2 does not affect the proliferation of tumor cells, the safety of their formulations on normal cells was still unknown. We incubated different concentrations of rSEC2 and its formulations with L929 cells, a mouse fibroblast cell line, and investigated their effects on cell growth using the CCK-8 assay. rSEC2 and its formulations maintained high cell compatibility across a wide range of rSEC2 concentrations from 0.001 to 10 μg/mL (Fig. 2K). We injected healthy mice with rSEC2 and its formulations at a dose of 4 mg/kg to investigate their hepatotoxicity and nephrotoxicity. Neither rSEC2 nor its formulations caused significant differences in AST, ALT, CREA, and BUN levels compared to the healthy group and PBS group (Fig. 2L−O), indicating that the formulations were safe at this dose.

3.3. Pulmonary tumor accumulation effect of i.v. biomimetic liposomes

The affinity of TSLs for different cells was initially investigated. HT29, L929, and RAW264.7 cell lines were used as controls to investigate the affinity of TSL for 4T1 cells. To facilitate the visualization of the formulation, we prepared a rSEC2 (GS) with sfGFP fused to the C-terminus to make TSL have green fluorescence and used it to prepare rSEC2 liposomes (GSL) and biomimetic liposomes (TGSL) with green fluorescence. Only 4T1 tumor cells recruited a large number of green fluorescent formulations that adhered to the cell surface, while the rest of the cells did not (Fig. 3A and B), indicating that TSL has a strong affinity for homologous tumor cells.

Then, GS, GSL, and TGSL were respectively injected intravenously into model mice to observe their *in vivo* organ targeting. Unexpectedly, all formulations were more distributed in the liver and kidneys than in the lung though TGSL was more distributed in the lung compared to the others (Fig. 3C and D). Although the hybridization of homologous tumor cell membranes can enhance the affinity of liposomes for the target cells, it is challenging to determine the *in vivo* tumor targeting properties of the formulation.

Given the abundance of capillaries in the lung, particles with larger diameters within the bloodstream are prone to be trapped in the lung[57]. We postulated that larger-diameter liposomes were more likely to be blocked in the lung. The empty liposomes with a diameter of ∼800 nm (SL-800) were separated using a Sephadex gel column to prepare large-diameter biomimetic liposomes (TSL-800, Fig. 3E and F). Meanwhile, in pursuit of more efficacious tumor chemoimmunotherapy, we prepared paclitaxel liposomes (PLs) using the reverse evaporation method and subsequently isolated ∼800 nm liposomes using the same technique to fabricate biomimetic liposomes (TSPL, Fig. 3E and F). The zeta potentials of SL, SL-800, TSL-800, and TSPL all ranged from −15 to −20 mV (Fig. 3G), indicating their stability. Additionally, the submicron liposomes, including SL-800, TSL-800, and TSPL, also displayed standard normal-size distribution (Fig. 3H). Similarly, we administered the formulations (GS, GSL, GSL-800, and TGSL-800) loaded sfGFP fused SEC2 to observe their *in vivo* distribution.

In the model mice, both GS and GSL were still distributed in the liver and kidneys, whereas GSL-800 and TGSL-800 exhibited a higher distribution in the lung (Fig. 3I and J). Furthermore, healthy mice were administered TGSL-800 to investigate whether its high pulmonary targeting was tumor-specific, revealing that TGSL-800 still exhibited a high distribution in the lung (Fig. 3I and J). To quantitatively analyze the pulmonary retention of various formulations, the amount of SEC2 in lung tissue was

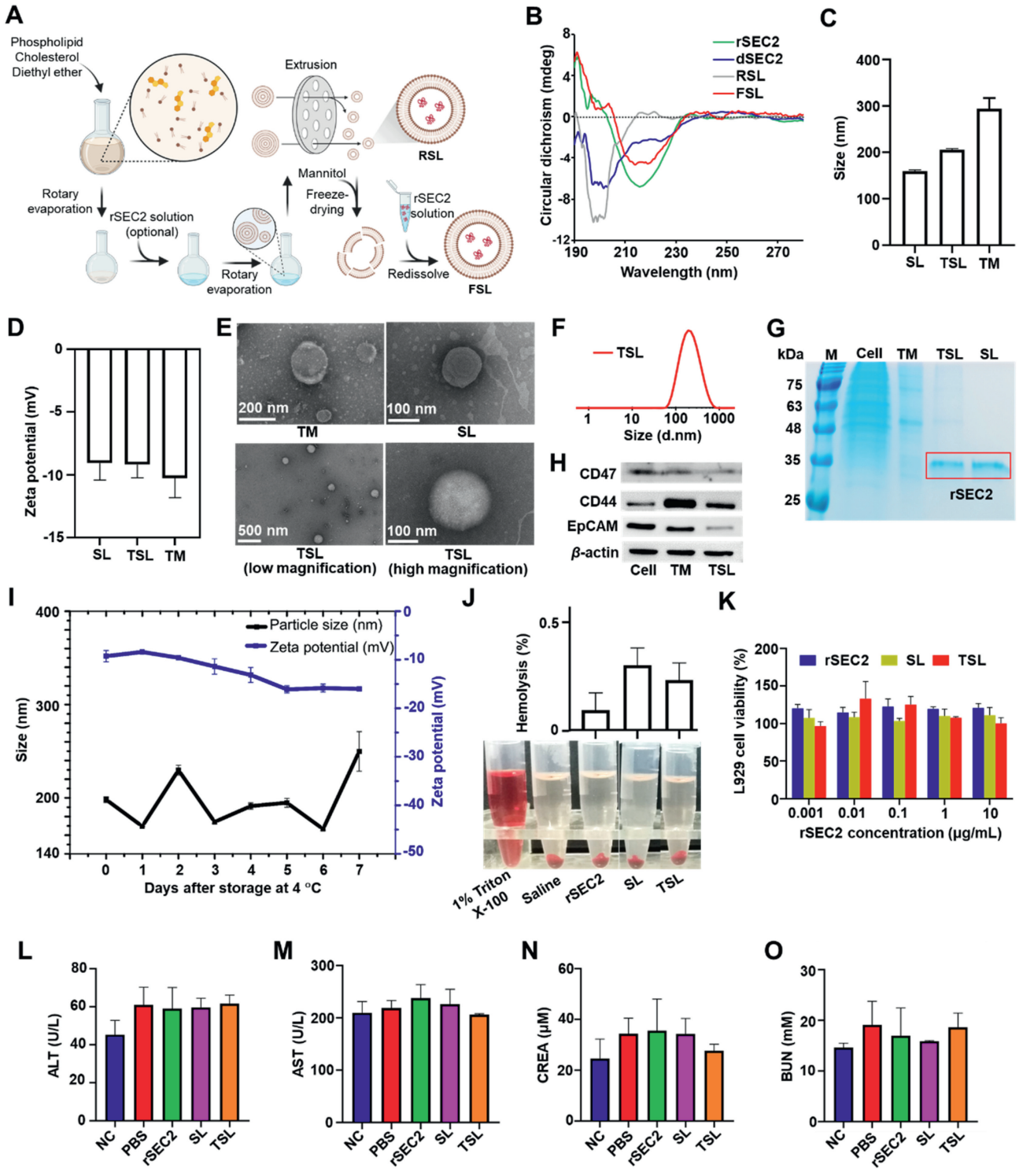

Figure 2 Preparation, characteristics, and safety of SLs and TSLs. (A) Process flow of rSEC2 liposome preparation by reverse evaporation (RSLs) and freeze-drying (DSLs) methods. (B) The CD spectrum of rSEC2, dSEC2, RSLs, and DSLs. Size (C), zeta potential (D), and TEM images (E) of 4T1 cell membranes (TMs), SLs and TSLs. The size distribution (F), SDS-PAGE (G), and Western blotting images (H) of TSLs. (I) The changes in particle size and zeta potential of TSLs within a week at 4 °C. (J) The hemolysis rate of rSEC2, SLs, and TSLs. (K) The L929 cell viability after treatment with various concentrations of rSEC2, SLs, and TSLs. ALT (L), AST (M), CREA (N), and BUN (O) levels in mice serum after receiving i.v. TSLs. Data are presented as mean ± SD ($n = 3$).

detected using ELISA. The rSEC2 concentration in the lung tissues of mice administered with GS and GSL was nearly identical, whereas the rSEC2 levels in the lung of mice administered with GSL-800 and TGSL-800 approximately doubled, indicating that an increase in particle size was a key factor in enhancing the lung targeting of biomimetic liposomes (Fig. 3K). However, the lung targeting induced by particle size was not specifically tumor-targeted, as TGSL-800 still exhibited high distribution in the lungs of the healthy group. Additionally, the rSEC2 content in the TGSL-800 group was significantly higher than that in the GSL-800 group, suggesting that the hybridization of tumor cell membranes further enhanced the lung-blocking rate due to the membrane proteins on the surface of biomimetic liposomes (Fig. 3K).

3.4. High antitumor effect of TSPLs

The metastatic lung cancer model was established after 4T1 cells were i.v. Injected into the mice (Fig. 4A). No deaths occurred in any group of mice throughout the entire experimental process. On Day 21, the lung of the model group was tumid with many tumor nodes and hemorrhage compared to the smooth and pink lungs of healthy mice (Fig. 4B). Furthermore, the lung weight of the model group was much larger than the healthy lung (Fig. 4B and C); each treatment group showed a reduction in lung weight increase caused by modelling, while the order of efficacy was TSPLs $>$ PLs $>$ TSL-800 $\approx$ SL-800 $>$ SLs $\approx$ rSEC2, indicating the superiority of the combination of large-sized liposomes, chemotherapy drugs, tumor cell membranes, and immune modulators in combating metastatic lung cancer (Fig. 4C). Moreover, the H&E staining images of lung tissue also demonstrated the antitumor effect of TSPLs; dense cancer cells and a large number of infiltrating inflammatory cells were observed in the model group; rSEC2, SL, SL-800 and TSL-800 groups showed improvement in the structure of the cancerous lung, while the pathological sections of PL showed fewer cancer cells and inflammatory infiltrates compared to the above four groups; the mice treated with TSPLs had been greatly modified (Fig. 4D).

As an important marker of apoptosis, TUNEL was used for lung tissue staining. Unlike the aforementioned results, the PL group showed a higher proportion of apoptosis, which was consistent with the anti-cancer mechanism of paclitaxel. Importantly, rSEC2 administration alone was able to cause apoptosis in lung cells, indicating its immune regulatory effect. The TSPL group showed the highest proportion of apoptosis among all SEC2 formulations, although it was lower than the PL group, which might be due to the stimulation of lymphocyte proliferation by SEC2 for anti-tumor purposes, while paclitaxel was a specific chemotherapeutic drug (Fig. 4D).

3.5. Low systemic immune response of TSPLs

Meanwhile, we focused on the systemic immune response caused by various SEC2 formulations, which was the main limiting factor for the anticancer effect of SEC2. The spleen index is an important parameter for evaluating the degree of spleen enlargement and the intensity of systemic immune response. Although TSPLs achieved the best antitumor effects, their spleen index was much lower than that of the rSEC2 and SL groups. In addition, we found that the large-sized liposome groups, including SL-800, TSL-800, and TSPL, had similarly low spleen indexes (Fig. 4E), indicating that the lung-targeted accumulation of SEC2 caused by particle size was the key to reducing systemic immune response.

The exploration of the WBC in whole blood also proved that large-sized liposomes (SL-800, TSL-800, and TSPLs) led to limited systemic immune responses (Fig. 4F), thereby reducing the side effects of SEC2. Together, we have shown that the hybrid submicron SEC2-paclitaxel liposome specifically accumulates in the lung, thereby avoiding a systemic cytokine storm that may be caused by the superantigen SEC2.

3.6. Local immune response enhanced by TSPLs

As an immune modulator, SEC2 directly acts on MHC-II molecules without being processed by antigen-presenting cells (APC), leading to T cell proliferation and secretion of inflammatory factors, resulting in antitumor immunity[58]. IL-4 is a multifunctional cytokine secreted by T_H2 cells that has antitumor effects and enhances immune function, playing an important role in the development of various tumors[59]. IL-2 is a classic antitumor factor secreted by iNKT cells and is a key molecule that promotes the proliferation and differentiation of T cells; its main function is to promote the expansion and function of lymphocytes, including T cells and natural killer cells, thereby enhancing their antitumor ability[60]. IFN-γ is the only type II interferon and is a hallmark cytokine produced by T_H1 cells, $CD8^+$ T cells, etc., exerting antitumor effects by promoting macrophage activation, upregulating the expression of antigen processing and presentation molecules, promoting the growth and activation of T_H1 cells and enhancing the function of NK cells[61]. IL-10 is traditionally considered to be an anti-inflammatory and immunosuppressive cytokine, but recent studies have shown that it can prevent dendritic cell-mediated apoptosis of $CD8^+$ T cells by regulating IFN-γ, thereby exerting antitumor effects[62].

The levels of inflammatory factors in the lung and spleen were quantified by ELISA to evaluate the local immune response. As expected, TSPLs caused the highest levels of cytokines in the lung, including IFN-γ, IL-4, IL-2, and IL-10 (Fig. 5A). However, rSEC2 and SLs caused no significant difference in cytokine levels compared with the model group except for IL-10, indicating that low pulmonary retention mediated local antitumor immunity in the lung was insufficient (Fig. 5A). The spleen of each group showed different cytokine profiles from the lungs; SLs caused the highest levels of cytokines in the spleen, not TSPLs (Fig. 5B), again demonstrating the high local distribution of TSPLs in the lung. Nonetheless, the formulations of large particle size still caused a moderate increase in spleen cytokines, which could be because the spleen is an important immune organ with a large number of lymphocytes, and a strong local immune response in the lungs may lead to activated T cells being transported to the spleen through the circulatory system, thereby causing immune activation in the spleen.

Tumor-associated macrophages (TAM) are closely associated with the occurrence and development of tumors[63]. M1 and M2 macrophages represent states of immune promotion and suppression, respectively, while malignant tumor cells induce macrophage polarization towards the M2 phenotype to facilitate tumor immune evasion[63]. An effective antitumor immune strategy involves reversing the polarization of macrophages from M2 to M1 state[64]. F4/80 is a surface antigen of mature macrophages, while CD206 is a typical surface antigen of M2 macrophages[63]. To investigate the effects of SEC2 on the polarization state of lung tumor-associated macrophages, F4/80 and CD206 were stained to label immunofluorescence. rSEC2 and its various formulations led to a decrease

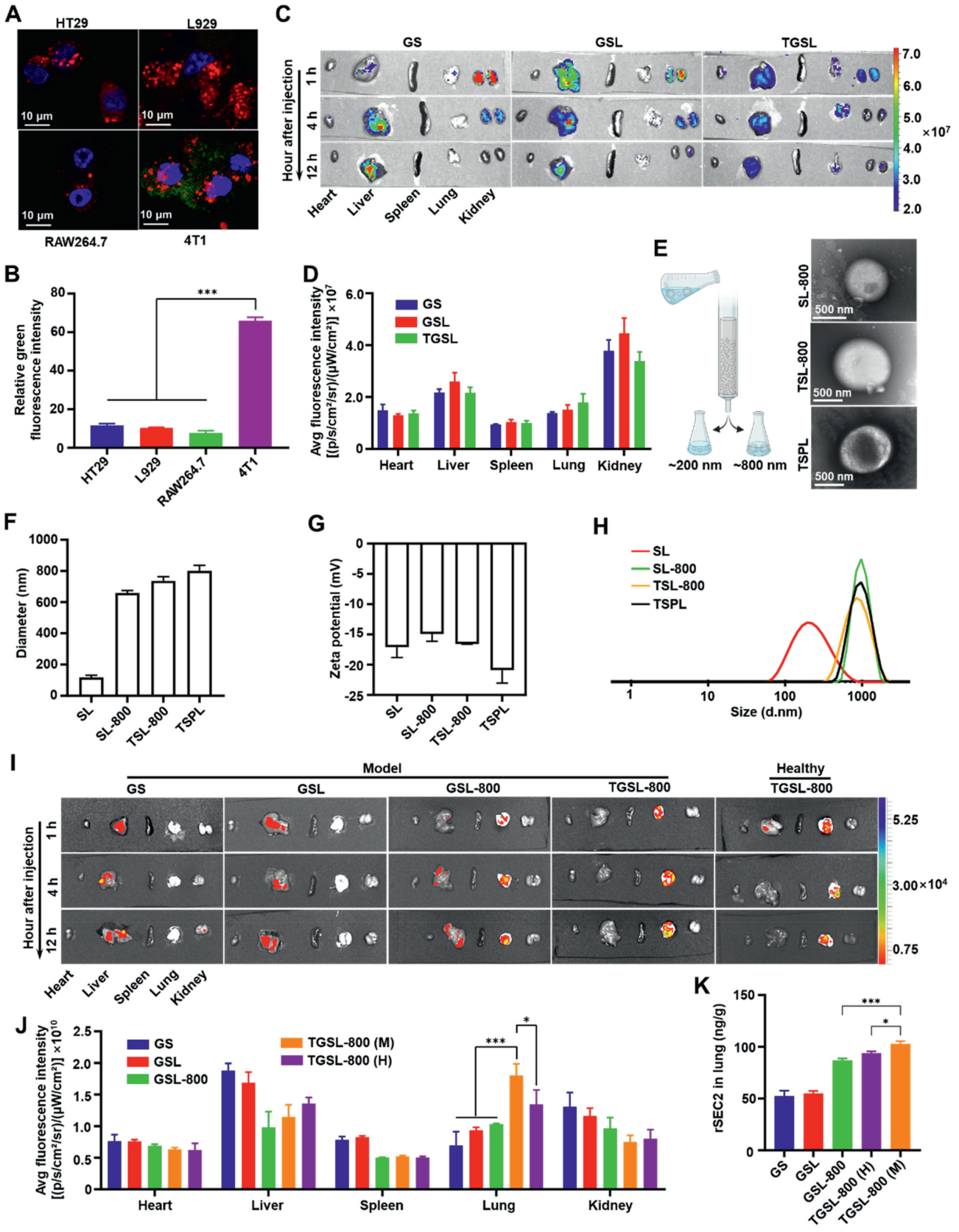

Figure 3 Cellular targeting and organ targeting of various formulations. Co-localization images (A) and semi-quantitative fluorescence intensity analysis (B) of TGSLs with HT29, L929, RAW264.7, and 4T1 cells; the cell nucleus, cell membranes, and TGSLs are labeled in blue, red, and green fluorescence, respectively. The main organs IVIS images (C) of mice and semi-quantitative fluorescence intensity analysis (D) after injection of GS, GSLs, and TGSLs. (E) Isolation of large particle size liposomes and TEM images of SL-800, TSL-800, and TSPL. Size (F) and

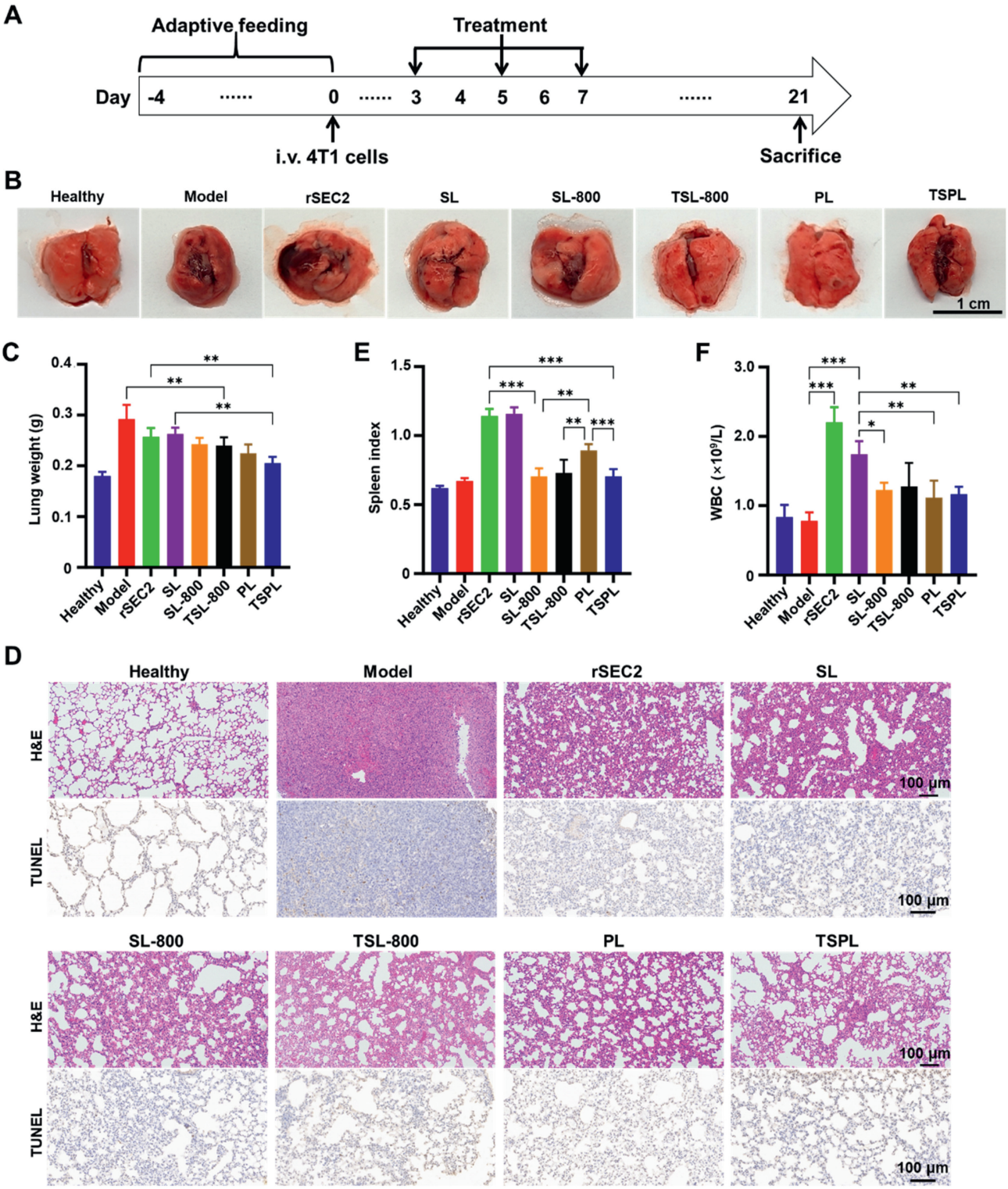

Figure 4 Antitumor effects of formulations. (A) Experimental procedure of the pharmacodynamic study. Appearance (B) and weight of the lungs (C) of the different groups. (D) H&E and TUNEL stained images of the lung tissue sections of the various groups. Spleen index (E) and WBC (F) of the various groups. Data are presented as mean ± SD ($n = 7$), *$P < 0.05$, **$P < 0.01$, ***$P < 0.001$.

zeta potential (G) and size distribution (H) of SLs, SL-800, TSL-800, and TSPL. The main organs IVIS images (I) of mice and semi-quantitative fluorescence intensity analysis (J) after injection of GS, GSLs, GSL-800, and TGSL-800. (K) The rSEC2 contents in the lungs of mice after injection of various formulations; H and M represent the healthy and model mice, respectively. Data are presented as mean ± SD ($n = 3$), *$P < 0.05$, ***$P < 0.001$.

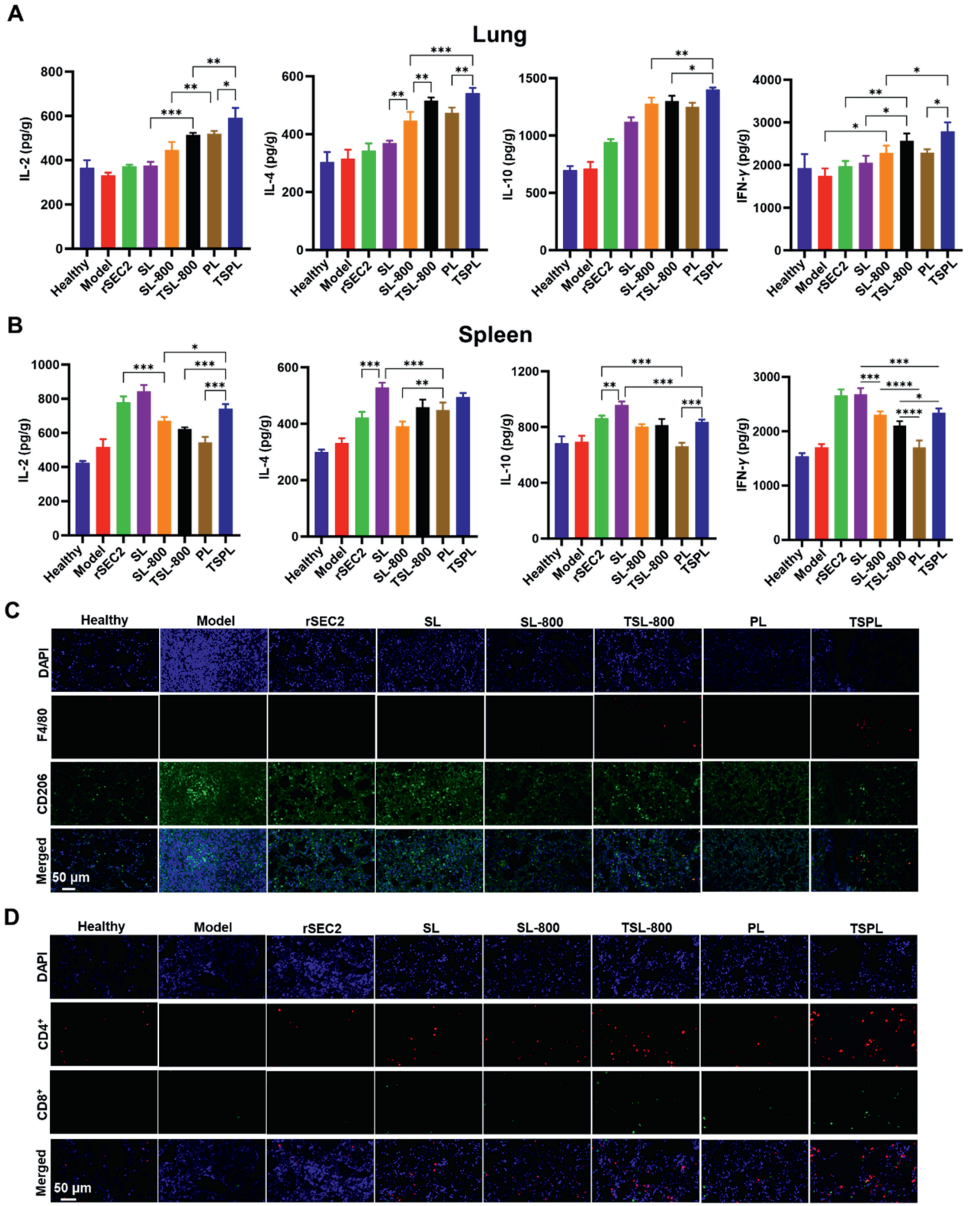

Figure 5 Local immunological effects on spleen and lung formulations. Cytokines (IL-2, IL-4, IL-10, IFN-γ) levels in the spleen (A) and lung (B) of various groups. (C) F4/80 and CD206 stained fluorescent images of the lung tissue sections of the various groups; the cell nucleus, F4/80, and CD206 are labeled in blue, red, and green, respectively. (D) CD4 and CD8 stained fluorescent images of the lung tissue sections of the various groups; the cell nucleus, $CD4^+$ T cells, and $CD8^+$ T cells are labeled in blue, red, and green, respectively. Data are presented as mean ± SD ($n = 4$), $^*P < 0.05$, $^{**}P < 0.01$, $^{***}P < 0.001$.

in the ratio of $CD206^+$ cells, while large particle size liposomes caused an increase in $F4/80^+$ cells (Fig. 5C), with TSPLs resulting in the highest $F4/80^+$ ratio and a lower $CD206^+$ ratio (Figs. 5C and 6A and B). This indicated that SEC2 effectively reversed the M2 to M1 polarization of macrophages, and the combination of lung targeting and paclitaxel further enhanced the reversal capability of TSPLs.

The host immune system can eliminate tumor cells through $CD8^+/CD4^+$ cytotoxic T lymphocytes. $CD8^+$ T cells are effector cells of tumor-specific immune responses, while $CD4^+$ T cells help generate $CD8^+$ T cells. TSPLs stimulated the immune system to generate the highest number of $CD4^+/CD8^+$ T cells in the lung compared to other groups (Fig. 5D). TSPL had a higher level of $CD4^+/CD8^+$ T cell ratios compared to TSL-800 (Fig. 6C and D), which may be attributed to the additional immune response caused by the fragmentation of dead tumor cells induced by paclitaxel.

4. Discussion

The treatment strategy for lung metastasis of cancer has been continuously concerned[65,66]. Although immune checkpoints and CAR-T are the main strategies for antitumor immunity, the simple and effective antitumor immune agent of immune modulators cannot be ignored. More and more clinical data show that the combination of chemotherapy and immunotherapy is more practical, so the integration of chemotherapy and immunotherapy is expected[67]. SE, as a bacterial superantigen, is a highly effective immune modulator, but it is prone to cause a systemic immune response and inflammatory cytokine storm, which limits its application[58]. We discussed the use of biomembrane materials and size control to improve the lung targeting of SEC2 and the combination with paclitaxel for the chemoimmunotherapy of metastatic lung cancer.

Based on structural and functional differences, SEs are divided into multiple subtypes, such as SEA-SEE, SEG-SEI, SER, etc., and we have selected a well-studied and less toxic SEC2[36]. We employed *E. coli* to produce SEC2 protein and obtained highly purified and active recombinant SEC2. This approach provides an alternative for potential industrial production in the future. The preparation process of liposomes affects the activity of protein drugs, as contact with organic solvents leads to protein denaturation. The lyophilized liposomes reconstituted with an aqueous solution of SEC2 maintained the CD spectrum of the active SEC2, while the reverse evaporation-prepared SEC2 liposomes lost their original CD spectrum characteristics. During the observation of the changes in particle size and zeta potential of TSL over 7 days, an interesting phenomenon was the zeta potential gradually decreased from −10 to −15 mV within 5 days and then stabilized. We attribute this phenomenon to minor rearrangement of the hybridized liposome membranes and their surface cell appendages

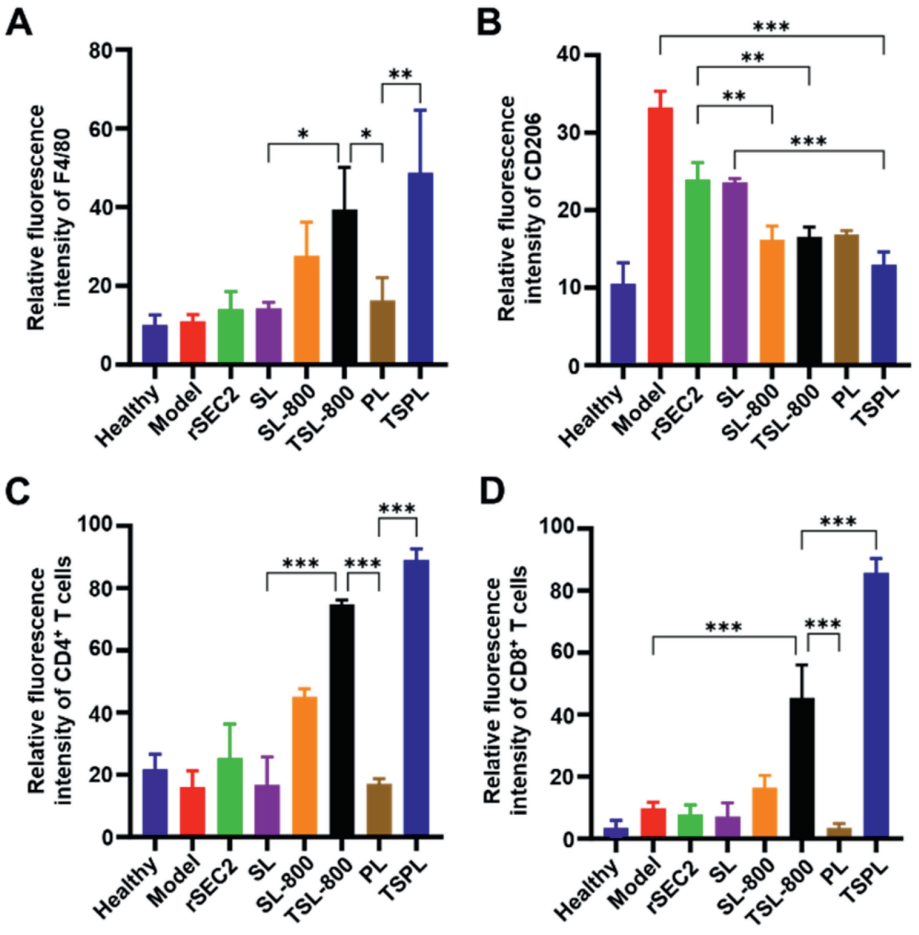

Figure 6 Semi-quantitative analyses of immunofluorescence images. The relative fluorescence intensity of F4/80 (A), CD206 (B), $CD4^+$ T cells (C), and $CD8^+$ T cells (D) in the lung tissue sections of the various groups. Data are presented as mean ± SD ($n = 4$), $^*P < 0.05$, $^{**}P < 0.01$, $^{***}P < 0.001$.

(such as membrane proteins and glycoproteins). Although the mechanical force during the co-extrusion process is sufficient to cause the hybridization of phospholipid membranes, it seems unable to instantly stabilize the proteins on the cell membrane. The rearrangement of proteins on the TSL membrane may lead to the presence of additional negative charges on the membrane. Membrane rearrangement of liposomes leading to surface charge changes is very common in hybrid liposomes[68,69]. Due to the complexity of biomembranes, the surface charge of biomembranes (*e.g.*, cell membranes) hybrid liposomes is easily affected by membrane protein rearrangement[70].

In the initial design, we thought that the hybridization of the homologous tumor cell membrane could lead to the accumulation of biomimetic liposomes at the tumor site to solve the problem of SEC2 targeting. However, the biomimetic liposomes distributed more in the liver and kidneys, probably due to insufficient affinity of the homologous cell membrane. Given the diameter of the pulmonary capillaries[57], we separated the submicron liposomes SL-800 with a gel column and prepared the TSL-800, a tumor cell membrane hybrid formulation. Interestingly, both have high lung targeting efficiency and TSL-800 has stronger targeting ability than SL-800, indicating that the blocking of submicron liposomes in the lungs leads to lung targeting, while the hybridization of the homologous tumor cell membrane further improves its retention efficiency. In general, particles larger than 500 nm injected intravenously may pose a risk of pulmonary embolism, primarily due to the abundant pulmonary capillary network and its micron-sized diameter (5−10 μm)[71]. Nevertheless, the particles that can trigger pulmonary embolism are typically solid and rigid, while the submicron-sized biomimetic liposomes formulated in this study are a spherical membrane structure with fluidity and flexibility, which can be squeezed and deformed during their passage through the pulmonary capillaries[72,73], allowing blood to pass smoothly. In addition, we did not observe any organic lesions caused by them in healthy mice (Fig. 3F). The size of the drug delivery vehicle is an important parameter that determines the drug target, biodistribution, drug clearance pathway and rate, and consequently determines the expected therapeutic effects[26,74,75]. TSL ($\sim$200 nm) accumulated more in the liver and kidneys (Fig. 3C and D), which was not a satisfactory biodistribution. Liposomes with larger sizes were investigated for their lung-targeting properties. The submicron-sized liposomes ($\sim$800 nm) were proven to be the expected lung targeting, indicating that larger liposomes tend to accumulate in the lungs (Fig. 3I and J). Continuing to increase the liposome particle size may lead to higher lung targeting efficiency, but considering the stability of liposomes and the risk of pulmonary embolism, the scheme was not adopted. Intriguingly, although TSL-800 did not lead to a higher lung targeting rate compared to SL-800 in healthy mice, its accumulation in the lung of model mice was higher than that of SL-800 (Fig. 3J and K). This can be attributed to the affinity and adhesion of tumor cell membrane components carried by TSL-800 to homogenous cells.

As expected, TSL-800 effectively reduced lung tumor burden, and the SEC2-paclitaxel integrated lung targeting formulation, TSPL showed the best effect. Moreover, the submicron SEC2-paclitaxel liposomes hybridized with tumor cell membranes almost did not cause excessive systemic immune response, greatly reducing the side effects of SEC2, which solved the problem of difficulty in large-scale clinical use of superantigen drugs. We also explored the mechanism of TSPL-induced antitumor immunity. SEC2 directly acts on the MHC−II−TCR complex, causing multiple T cell activation and proliferation without APC presentation[76]. Therefore, rSEC2 should be released into the intercellular space to directly act on the cell surface. Although liposome-mediated intracellular delivery is well known[77], the submicron biomimetic liposomes prepared in this study are prone to membrane rupture or incomplete membrane fusion, releasing superantigens into the intercellular space during the penetration of liposomes into tumor tissues, which also is mentioned in previous reports[78,79]. However, some liposomes will mediate intracellular delivery of rSEC2 by endocytosis or complete membrane fusion, leading to the inactivation of the superantigens. Nevertheless, from the perspective of the final pharmacodynamic results, the intercellular superantigens released by the submicron biomimetic liposomes are sufficient to reverse the immunosuppressive microenvironment and mediate anti-tumor immune responses.

We found that SEC2 not only caused an increase in typical inflammatory factors in the lung but also led to an increase in IL-10, although the mechanism of IL-10 antitumor activity had only been clarified in recent years[62]. SEC2 also led to an increase in $CD4^+/CD8^+$ T cells, causing antitumor cellular immunity. Importantly, SEC2 reversed the polarization state of macrophages from immunosuppressive M2 to immunostimulatory M1. These results provide insights into clarifying the antitumor mechanism of TSPLs. Meanwhile, although TSPLs led to the highest level of antitumor immunity in the lung compared to other formulations, they did not lead to the highest level of immune response in the spleen, indicating that biomaterials and particle size jointly determine the efficient lung retention and low systemic immune response of TSPLs.

5. Conclusions

We propose a new strategy for lung tumor targeting, a submicron biomimetic liposome hybridized with the membrane of homologous tumor cells. This liposome is used to deliver both SEC2, a bacterial superantigen, and paclitaxel for lung metastasis chemoimmunotherapy. This therapy has been shown to have excellent antitumor effects. SEC2 mediates high levels of antitumor immunity in the lung while avoiding systemic immune responses and inflammatory storms, indicating that the biomaterial and its preparation strategy are suitable for protein-based immunomodulators in chemoimmunotherapy. In addition, the bacterial superantigen and its formulation preparation method we used are suitable for industrial production, thus having potential clinical transformation prospects.

Acknowledgments

The work was partially supported by the Medical Innovation Research Project (23SWAQ12), National Natural Science Foundation of China (82404486) and Beijing Natural Science Foundation (L232085, China).

Author contributions

Bochuan Yuan, Yiguang Jin and Fei Xie designed the research. Bochuan Yuan, Feng Zhang, Qiucheng Yan carried out the experiments and performed data analysis. Wanmei Wang, Zhangyu Li participated part of the experiments. Lina Du provided experimental drugs and quality control. Bochuan Yuan wrote the manuscript. Bochuan Yuan, Yiguang Jin and Fei Xie revised the manuscript. All of the authors have read and approved the final manuscript.

Conflicts of interest

The authors have no conflicts of interest to declare.

References

1. Leiter A, Veluswamy RR, Wisnivesky JP. The global burden of lung cancer: current status and future trends. *Nat Rev Clin Oncol* 2023;**20**: 624−39.
2. Mohammed TL, Chowdhry A, Reddy GP, Amorosa JK, Brown K, Dyer DS, et al. ACR Appropriateness Criteria® screening for pulmonary metastases. *J Thorac Imag* 2011;**26**:W1−3.
3. Zhang FY, Guo ZY, Li ZX, Luan H, Yu YY, Zhu AT, et al. Biohybrid microrobots locally and actively deliver drug-loaded nanoparticles to inhibit the progression of lung metastasis. *Sci Adv* 2024;**10**:eadn6157.
4. Cheng DC, Tian R, Pan TT, Yu Q, Wei L, Liyin JZ, et al. High-performance lung-targeted bio-responsive platform for severe colistin-resistant bacterial pneumonia therapy. *Bioact Mater* 2024; **35**:517−33.
5. Wang BL, Hu SQ, Teng Y, Chen JL, Wang HY, Xu YZ, et al. Current advance of nanotechnology in diagnosis and treatment for malignant tumors. *Signal Transduct Target Ther* 2024;**9**:200.
6. Chen L, Deng J, Yu AL, Hu YH, Jin B, Du PY, et al. Drug-peptide supramolecular hydrogel boosting transcorneal permeability and pharmacological activity *via* ligand-receptor interaction. *Bioact Mater* 2022;**10**:420−9.
7. Xu B, Zeng FJ, Deng JL, Yao LT, Liu SB, Hou HL, et al. A homologous and molecular dual-targeted biomimetic nanocarrier for EGFR-related non-small cell lung cancer therapy. *Bioact Mater* 2023;**27**: 337−47.
8. Wu ZJ, Chen L, Guo WY, Wang J, Ni HY, Liu JN, et al. Oral mitochondrial transplantation using nanomotors to treat ischaemic heart disease. *Nat Nanotechnol* 2024;**19**:1375−85.
9. Chen JJ, Ye ZF, Huang CF, Qiu M, Song DH, Li YM, et al. Lipid nanoparticle-mediated lymph node-targeting delivery of mRNA cancer vaccine elicits robust $CD8^+$ T cell response. *Proc Natl Acad Sci U S A* 2022;**119**:e2207841119.
10. Kon E, Elia U, Peer D. Principles for designing an optimal mRNA lipid nanoparticle vaccine. *Curr Opin Biotechnol* 2022;**73**:329−36.
11. Tenchov R, Bird R, Curtze AE, Zhou QQ. Lipid nanoparticles horizontal line from liposomes to mRNA vaccine delivery, a landscape of research diversity and advancement. *ACS Nano* 2021;**15**:16982−7015.
12. Deshpande PP, Biswas S, Torchilin VP. Current trends in the use of liposomes for tumor targeting. *Nanomedicine* 2013;**8**:1509−28.
13. Zhao PF, Wang S, Jiang JZ, Gao YR, Wang YW, Zhao YG, et al. Targeting lactate metabolism and immune interaction in breast tumor *via* protease-triggered delivery. *J Control Release* 2023;**358**:706−17.
14. Pitchaimani A, Nguyen TDT, Aryal S. Natural killer cell membrane infused biomimetic liposomes for targeted tumor therapy. *Biomaterials* 2018;**160**:124−37.
15. Fang RH, Gao WW, Zhang LF. Targeting drugs to tumours using cell membrane-coated nanoparticles. *Nat Rev Clin Oncol* 2023;**20**:33−48.
16. Jiang Y, Krishnan N, Zhou JR, Chekuri S, Wei XL, Kroll AV, et al. Engineered cell-membrane-coated nanoparticles directly present tumor antigens to promote anticancer immunity. *Adv Mater* 2020;**32**: e2001808.
17. Wang B, Yang PB, Ding YX, Qi HL, Gao Q, Zhang CX. Improvement of the biocompatibility and potential stability of chronicallyimplanted electrodes incorporating coating cell membranes. *ACS Appl Mater Inter* 2019;**11**:8807−17.
18. Oroojalian F, Beygi M, Baradaran B, Mokhtarzadeh A, Shahbazi MA. Immune cell membrane-coated biomimetic nanoparticles for targeted cancer therapy. *Small* 2021;**17**:e2006484.
19. Chen Z, Zhao PF, Luo ZY, Zheng MB, Tian H, Gong P, et al. Cancer cell membrane-biomimetic nanoparticles for homologous-targeting dual-modal imaging and photothermal therapy. *ACS Nano* 2016;**10**: 10049−57.
20. He ZH, Zhang YT, Feng NP. Cell membrane-coated nanosized active targeted drug delivery systems homing to tumor cells: a review. *Mater Sci Eng C Mater Biol Appl* 2020;**106**:110298.
21. Liu LZ, Pan DY, Chen S, Martikainen MV, Karlund A, Ke J, et al. Systematic design of cell membrane coating to improve tumor targeting of nanoparticles. *Nat Commun* 2022;**13**:6181.
22. Hu CM, Fang RH, Luk BT, Chen KN, Carpenter C, Gao WW, et al. 'Marker-of-self' functionalization of nanoscale particles through a top-down cellular membrane coating approach. *Nanoscale* 2013;**5**:2664−8.
23. Hu CM, Zhang L, Aryal S, Cheung C, Fang RH, Zhang LF. Erythrocyte membrane-camouflaged polymeric nanoparticles as a biomimetic delivery platform. *Proc Natl Acad Sci U S A* 2011;**108**: 10980−5.
24. Abra RM, Hunt CA. Liposome disposition *in vivo*. III. Dose and vesicle-size effects. *Biochim Biophys Acta* 1981;**666**:493−503.
25. Dadashzadeh S, Vali AM, Rezaie M. The effect of PEG coating on *in vitro* cytotoxicity and *in vivo* disposition of topotecan loaded liposomes in rats. *Int J Pharm* 2008;**353**:251−9.
26. Dhand C, Prabhakaran MP, Beuerman RW, Lakshminarayanan R, Dwivedi N, Ramakrishna S. Role of size of drug delivery carriers for pulmonary and intravenous administration with emphasis on cancer therapeutics and lung-targeted drug delivery. *RSC Adv* 2014;**4**:32673−89.
27. Borm P, Klaessig FC, Landry TD, Moudgil B, Pauluhn J, Thomas K, et al. Research strategies for safety evaluation of nanomaterials, part V: role of dissolution in biological fate and effects of nanoscale particles. *Toxicol Sci* 2006;**90**:23−32.
28. Zhang XK, Sun P, Bi R, Wang JP, Zhang N, Huang GH. Targeted delivery of levofloxacin-liposomes for the treatment of pulmonary inflammation. *J Drug Target* 2009;**17**:399−407.
29. Agnoletti M, Rodriguez-Rodriguez C, Klodzinska SN, Esposito TVF, Saatchi K, Morck Nielsen H, et al. Monosized polymeric microspheres designed for passive lung targeting: biodistribution and pharmacokinetics after intravenous administration. *ACS Nano* 2020;**14**:6693−706.
30. Duffett L, Castellucci LA, Forgie MA. Pulmonary embolism: update on management and controversies. *BMJ* 2020;**370**:m2177.
31. Yang Y, Zoulikha M, Xiao QQ, Huang FF, Jiang Q, Li XT, et al. Pulmonary endothelium-targeted nanoassembly of indomethacin and superoxide dismutase relieves lung inflammation. *Acta Pharm Sin B* 2023;**13**:4607−20.
32. Finck AV, Blanchard T, Roselle CP, Golinelli G, June CH. Engineered cellular immunotherapies in cancer and beyond. *Nat Med* 2022;**28**: 678−89.
33. Kennedy LB, Salama AKS. A review of cancer immunotherapy toxicity. *CA Cancer J Clin* 2020;**70**:86−104.
34. Lando PA, Hedlund G, Dohlsten M, Kalland T. Bacterial superantigens as anti-tumour agents: induction of tumour cytotoxicity in human lymphocytes by staphylococcal enterotoxin A. *Cancer Immunol Immunother* 1991;**33**:231−7.
35. Chen JY. Superantigens, superantigen-like proteins and superantigen derivatives for cancer treatment. *Eur Rev Med Pharmacol Sci* 2021;**25**: 1622−30.
36. Tuffs SW, Dufresne K, Rishi A, Walton NR, McCormick JK. Novel insights into the immune response to bacterial T cell superantigens. *Nat Rev Immunol* 2024;**24**:417−34.
37. Wan XC, Liu CP, Li M, Hong D, Li DM, Chen HX, et al. Staphylococcal enterotoxin C injection in combination with ascorbic acid promotes the differentiation of bone marrow-derived mesenchymal stem cells into osteoblasts *in vitro*. *Biochem Biophys Res Commun* 2008;**373**:488−92.
38. Brocke S, Gaur A, Piercy C, Gautam A, Gijbels K, Fathman CG, et al. Induction of relapsing paralysis in experimental autoimmune encephalomyelitis by bacterial superantigen. *Nature* 1993;**365**:642−4.
39. Ochi A, Migita K, Xu J, Siminovitch K. *In vivo* tumor immunotherapy by a bacterial superantigen. *J Immunol* 1993;**151**:3180−6.
40. Zhou JY, Liu L, Xu MK, Zhang HW, Zhang YX, Zhang CG. T-cell proliferation and antitumour activities of a truncated mutant of staphylococcal enterotoxin C2 with decreased cytokine secretion. *J Med Microbiol* 2013;**62**:451−6.

41. Krakauer T. Staphylococcal superantigens: pyrogenic toxins induce toxic shock. *Toxins* 2019;**11**:178.
42. Zemek RM, Anagnostou V, Pires da Silva I, Long GV, Lesterhuis WJ. Exploiting temporal aspects of cancer immunotherapy. *Nat Rev Cancer* 2024;**24**:480−97.
43. Emens LA, Ascierto PA, Darcy PK, Demaria S, Eggermont AMM, Redmond WL, et al. Cancer immunotherapy: opportunities and challenges in the rapidly evolving clinical landscape. *Eur J Cancer* 2017;**81**:116−29.
44. Wei J, Yang YY, Wang G, Liu M. Current landscape and future directions of bispecific antibodies in cancer immunotherapy. *Front Immunol* 2022;**13**:1035276.
45. Imani Fooladi AA, Halabian R, Mahdavi M, Amin M, Mahmoodzadeh Hosseini H. Staphylococcal enterotoxin B/texosomes as a candidate for breast cancer immunotherapy. *Tumour Biol* 2016;**37**:739−48.
46. Zhou P, Liang P, Dong BW, Yu XL, Han XJ, Wang Y, et al. Long-term results of a phase II clinical trial of superantigen therapy with staphylococcal enterotoxin C after microwave ablation in hepatocellular carcinoma. *Int J Hyperthermia* 2011;**27**:132−9.
47. Liu Y, Zhuang B, Yuan BC, Zhang H, Li JF, Wang WM, et al. Predatory bacterial hydrogels for topical treatment of infected wounds. *Acta Pharm Sin B* 2023;**13**:315−26.
48. Ahn S, Siddiqi MH, Aceituno VC, Simu SY, Yang DC. Suppression of MAPKs/NF-kappaB activation induces intestinal anti-Inflammatory action of ginsenoside Rf in HT-29 and RAW264.7 cells. *Immunol Investig* 2016;**45**:439−49.
49. Schmid-Burgk JL, Schmidt T, Kaiser V, Honing K, Hornung V. A ligation-independent cloning technique for high-throughput assembly of transcription activator-like effector genes. *Nat Biotechnol* 2013;**31**:76−81.
50. Yuan BC, Liu D, Guan X, Yan YC, Zhang JP, Zhang YP, et al. Piperazine ring formation by a single-module NRPS and cleavage by an alpha-KG-dependent nonheme iron dioxygenase in brasiliamide biosynthesis. *Appl Microbiol Biotechnol* 2020;**104**:6149−59.
51. Xiao ZM, Zhuang B, Zhang GL, Li M, Jin YG. Pulmonary delivery of cationic liposomal hydroxycamptothecin and 5-aminolevulinic acid for chemo-sonodynamic therapy of metastatic lung cancer. *Int J Pharm* 2021;**601**:120572.
52. Liu J, Deng Y, Fu D, Yuan Y, Li QL, Shi L, et al. Sericin microparticles enveloped with metal-organic networks as a pulmonary targeting delivery system for intra-tracheally treating metastatic lung cancer. *Bioact Mater* 2021;**6**:273−84.
53. Souvorov A, Agarwala R, Lipman DJ. SKESA: strategic k-mer extension for scrupulous assemblies. *Genome Biol* 2018;**19**:153.
54. Willingham SB, Volkmer JP, Gentles AJ, Sahoo D, Dalerba P, Mitra SS, et al. The CD47-signal regulatory protein alpha (SIRPα) interaction is a therapeutic target for human solid tumors. *Proc Natl Acad Sci U S A* 2012;**109**:6662−7.
55. Ponta H, Sherman L, Herrlich PA. CD44: from adhesion molecules to signalling regulators. *Nat Rev Mol Cell Biol* 2003;**4**:33−45.
56. Li D, Guo XL, Yang K, Yang YN, Zhou WL, Huang Y, et al. EpCAM-targeting CAR-T cell immunotherapy is safe and efficacious for epithelial tumors. *Sci Adv* 2023;**9**:eadg9721.
57. Guelfi S, Hodivala-Dilke K, Bergers G. Targeting the tumour vasculature: from vessel destruction to promotion. *Nat Rev Cancer* 2024;**24**:655−75.
58. Thammavongsa V, Kim HK, Missiakas D, Schneewind O. Staphylococcal manipulation of host immune responses. *Nat Rev Microbiol* 2015;**13**:529−43.
59. Chan WL, Pejnovic N, Liew TV, Hamilton H. Predominance of Th2 response in human abdominal aortic aneurysm: mistaken identity for IL-4-producing NK and NKT cells?. *Cell Immunol* 2005;**233**:109−14.
60. Cao L, Morgun E, Genardi S, Visvabharathy L, Cui YY, Huang HC, et al. METTL14-dependent m^6A modification controls iNKT cell development and function. *Cell Rep* 2022;**40**:111156.
61. Zhang BB, Zeng MN, Zhang QQ, Wang R, Jia JF, Cao B, et al. *Ephedrae herba* polysaccharides inhibit the inflammation of ovalbumin induced asthma by regulating Th1/Th2 and Th17/Treg cell immune imbalance. *Mol Immunol* 2022;**152**:14−26.
62. Qiao J, Liu ZD, Dong CB, Luan Y, Zhang AL, Moore C, et al. Targeting tumors with IL-10 prevents dendritic cell-mediated $CD8^+$ T cell apoptosis. *Cancer Cell* 2019;**35**:901−15.e4.
63. Li DM, Zhang T, Guo Y, Bi C, Liu M, Wang G. Biological impact and therapeutic implication of tumor-associated macrophages in hepatocellular carcinoma. *Cell Death Dis* 2024;**15**:498.
64. Zhao MM, Cheng XH, Shao PW, Dong Y, Wu YJ, Xiao L, et al. Bacterial protoplast-derived nanovesicles carrying CRISPR-Cas9 tools re-educate tumor-associated macrophages for enhanced cancer immunotherapy. *Nat Commun* 2024;**15**:950.
65. Shi XL, Wang XY, Yao WT, Shi DM, Shao XH, Lu ZQ, et al. Mechanism insights and therapeutic intervention of tumor metastasis: latest developments and perspectives. *Signal Transduct Target Ther* 2024;**9**:192.
66. Altorki NK, Markowitz GJ, Gao DC, Port JL, Saxena A, Stiles B, et al. The lung microenvironment: an important regulator of tumour growth and metastasis. *Nat Rev Cancer* 2019;**19**:9−31.
67. Shanafelt TD, Wang XV, Kay NE, Hanson CA, O'Brien S, Barrientos J, et al. Ibrutinib-rituximab or chemoimmunotherapy for chronic lymphocytic leukemia. *N Engl J Med* 2019;**381**:432−43.
68. Marsden HR, Tomatsu I, Kros A. Model systems for membrane fusion. *Chem Soc Rev* 2011;**40**:1572−85.
69. Marusic N, Otrin L, Rauchhaus J, Zhao ZL, Kyrilis FL, Hamdi F, et al. Increased efficiency of charge-mediated fusion in polymer/lipid hybrid membranes. *Proc Natl Acad Sci U S A* 2022;**119**:e2122468119.
70. Evers MJW, van de Wakker SI, de Groot EM, de Jong OG, Gitz-Francois JJJ, Seinen CS, et al. Functional siRNA delivery by extracellular vesicle-liposome hybrid nanoparticles. *Adv Healthc Mater* 2022;**11**:e2101202.
71. Liu F, Hutchinson R. Visible particles in parenteral drug products: a review of current safety assessment practice. *Curr Res Toxicol* 2024;**7**:100175.
72. Zhao J, Mao SR. Chapter three: tuning the membrane fluidity of liposomes for desirable *in vivo* fate with enhanced drug delivery. *Adv Biomembranes Lipid Self-Assembly* 2021;**34**:67−106.
73. Uchiyama K, Nagayasu A, Yamagiwa Y, Nishida T, Harashima H, Kiwada H. Effects of the size and fluidity of liposomes on their accumulation in tumors: a presumption of their interaction with tumors. *Int J Pharmaceut* 1995;**121**:195−203.
74. Qiao Q, Liu X, Yang T, Cui KX, Kong L, Yang CL, et al. Nanomedicine for acute respiratory distress syndrome: the latest application, targeting strategy, and rational design. *Acta Pharm Sin B* 2021;**11**:3060−91.
75. Decuzzi P, Godin B, Tanaka T, Lee SY, Chiappini C, Liu X, et al. Size and shape effects in the biodistribution of intravascularly injected particles. *J Control Release* 2010;**141**:320−7.
76. Irwin MJ, Hudson KR, Fraser JD, Gascoigne NRJ. Enterotoxin residues determining T-cell receptor Vβ binding specificity. *Nature* 1992;**359**:841−3.
77. Paasonen L, Sipila T, Subrizi A, Laurinmaki P, Butcher SJ, Rappolt M, et al. Gold-embedded photosensitive liposomes for drug delivery: triggering mechanism and intracellular release. *J Control Release* 2010;**147**:136−43.
78. He HS, Lu Y, Qi JP, Zhu QG, Chen ZJ, Wu W. Adapting liposomes for oral drug delivery. *Acta Pharm Sin B* 2019;**9**:36−48.
79. Wang BH, Zhang HF, An JY, Zhang YW, Sun LL, Jin YJ, et al. Sequential intercellular delivery nanosystem for enhancing ROS-induced antitumor therapy. *Nano Lett* 2019;**19**:3505−18.